Electrochemical performance and stability of Sr-doped LaMnO$_3$-infiltrated yttria stabilized zirconia oxygen electrode for reversible solid oxide fuel cells

Hui Fan · Minfang Han

Abstract Porous Sr-doped lanthanum manganite–yttria stabilized zirconia (LSM–YSZ) oxygen electrode is prepared by an infiltration process for a reversible solid oxide fuel cell (RSOFC). X-ray diffraction and SEM analysis display that perovskite phase LSM submicro particles are evenly distributed in the porous YSZ matrix. Polarization curves and electrochemical impedance spectra are conducted for the RSOFC at 800 and 850 °C under both SOFC and SOEC modes. At 850 °C, the single cell has the maximum power density of ∼726 mW/cm^2 under SOFC mode, and electrolysis voltage of 1.35 V at 1 A/cm^2 under SOEC mode. Fuel cell/water electrolysis cycle shows the cell has good performance stability during 6 cycles, which exhibits the LSM–YSZ oxygen electrode has high electrochemical performance and good stability. The results suggest that network-like LSM–YSZ electrode made by infiltration process could be a promising oxygen electrode for high temperature RSOFCs.

Keywords Reversible solid oxide fuel cell · Solid oxide electrolysis cell · Infiltration · Strontium-doped lanthanum manganite

1 Introduction

A reversible solid oxide fuel cell (RSOFC) is an electrochemical device which can be operated at high temperature under both power generation mode and electrolysis mode (Gopalan et al. 2006; Tao et al. 2009; Jung et al. 2012). In power generation mode, the RSOFCs produce electricity directly from electrochemically oxidizing fuel. While, in electrolysis mode, power is applied to the cell and the RSOFC acts as a solid oxide electrolysis cell (SOEC). RSOFCs can be integrated with renewable production of electricity and hydrogen when power generation and steam electrolysis are coupled in a system (Chen et al. 2010; Rao et al. 2012). With the RSOFC, fuel such as hydrogen can be used to produce electricity by an SOFC, and the electricity can then be used to produce hydrogen from water electrolysis.

Studies have shown that the state-of-the-art SOFC materials could be directly employed in an SOEC, with Ni/YSZ (8 mol% Y$_2$O$_3$ stabilized ZrO$_2$) cermet hydrogen electrode, YSZ oxygen-ion conducting electrolyte, and perovskite LSM (Sr-doped LaMnO$_3$) and/or LSM–YSZ oxygen electrode (Kim-Lohsoontorn et al. 2010; Chen et al. 2012a). Delamination at the oxygen electrode/electrolyte interface was reported to be one of the most important problems causing the performance degradation and cell failure for an SOEC (Keane et al. 2012; Kim et al. 2013). Virkar (2010) reported that the high oxygen pressure developed inside the electrolyte near the air electrode could lead to the delamination of the oxygen electrode. Chen et al. (2010) systematically studied the polarization behavior and delamination mechanism of LSM oxygen electrode under SOEC operation conditions. They characterized the oxygen electrode and electrolyte interface by SEM and the results indicated that the delamination of LSM oxygen electrode was caused by the disintegration of

H. Fan · M. Han (✉)
Union Research Center of Fuel Cell, School of Chemical & Environment Engineering, China University of Mining & Technology (Beijing), Beijing 100083, China
e-mail: hanminfang@sina.com

the LSM particles at the oxygen electrode and electrolyte interfaces (Chen and Jiang 2011). Knibbe et al. (2009) studied the degradation behavior of SOEC under high current densities and suggested that the degradation was ascribed to the nucleation and growth of oxygen clusters in the YSZ grain boundaries near the oxygen electrode. Keane et al. (2012) fabricated symmetric air/LSM//YSZ//LSM/air cells and measured electrical performance degradation with time at various applied voltage ranging from 0 to 0.8 V with respect to OCV. After test, a developed weak oxygen electrode–electrolyte interface resulting from the delamination between the oxygen electrode and electrolyte was observed. Microstructural analysis of the oxygen electrode–electrolyte interface indicated the formation of lanthanum zirconate and morphological changes at the interface.

In studies on SOFC, by depositing active ionic/electronic-conductive nano-particles on porous electrode surface, the number of oxygen reduction reaction sites could be largely increased. It thereby enhanced the active triple phase boundary (TPB) zone, lowered the area specific resistance (ASR), and improved the electrochemical performance of SOFCs (Jiang 2012; Fu et al. 2012; Kiebach et al. 2013). LSM particles infiltrated into pre-sintered porous YSZ network could create a high density of active sites for the oxygen reduction reaction (Sholklapper et al. 2006). The Ni–YSZ/YSZ/LSM–YSZ cell fabricated by infiltration process achieved an open circuit voltage at $\sim$1.1 V and maximum power density at $\sim$0.27 W/cm^2 at 923 K. In addition, the infiltrated cell had a polarization resistance of 2.9 $\Omega \cdot$cm^2, which was strikingly smaller than 110 $\Omega \cdot$cm^2 of the cell prepared by conventional method (Sholklapper et al. 2006). Yang et al. (2010) prepared porous LSM–YSZ oxygen electrode by an infiltration method for high-temperature water electrolysis. After electrolyzing at 800 °C and a current density of 0.33 A/cm^2 for 50 h with 50 vol% AH (absolute humidity, the vol% of humidity in the total gas volume), there was no deterioration of the electrochemical performance for the LSM-infiltrated cell and as well as the delamination of oxygen electrode from electrolyte. ASR of the LSM-infiltrated cell was substantially lower than that of the cell with LSM–YSZ oxygen electrode made by a screen printing method. Chen et al. (2012b) also indicated that LSM-infiltrated LSM–YSZ composite oxygen electrode showed high electrocatalytic activity and good stability under SOEC operation. By infiltrating porous YSZ matrix with LSM nitrate solution, the electrode heat-treated at 900 °C exhibited a low electrode polarization resistance of 0.21 $\Omega \cdot$cm^2 at 800 °C.

In this paper, the electrochemical performance of a H$_2$ electrode-supported Ni–YSZ/YSZ/LSM–YSZ RSOFC with LSM infiltrated oxygen electrode was investigated under both fuel cell and electrolysis modes. The fuel cell/water electrolysis cycle performance of the cell at 0.4 A/cm^2 was carried out as well for evaluating the cell stability.

2 Experimental

RSOFCs, which consisted of Ni–YSZ hydrogen electrode supports, thin YSZ electrolytes, and infiltrated LSM–YSZ oxygen electrodes, were fabricated by tape casting and infiltration technique. For fabricating the Ni–YSZ electrode, powders of NiO, YSZ (8 mol% yttria stabilized zirconia, with a median particle size of 0.114 μm) and graphite (Furunda Zirconium Material Co., Ltd., China) pore former were mixed and ball-milled in a weight ratio of 50:50:10 with appropriate amounts of ethanol-butanone solvent, caster oil dispersant, dibutyl phthalate (DBP) plasticizer, and polyvinyl butyral (PVB) binder. A two-stage milling process (Liu et al. 2010) was adopted. Firstly, NiO and YSZ powders were dispersed in mixed solvent and dispersant via ball-milling for 15–20 h. Secondly, a homogenous mixture including remaining solvent, plasticizer, and binder formed by thermal dissolution was added, and the resultant slurry was then ball milled for another 24 h before adding the last constituent of graphite. For YSZ electrolytes, the same way of tape casting as in the case of NiO–YSZ substrates was used excepted for no addition of NiO and graphite powders. Porous YSZ layers were prepared with higher ratio of pore formers. Through previous study on different weight ratios of graphite to YSZ, 50 wt% was thought as an optimal proportion. A tape casting machine (DR-150, made in Japan) was used for separately casting the NiO–YSZ layer, the electrolyte, and the porous YSZ electrode. These tapes were dried in air at room temperature for 12 h. One sheet of NiO–YSZ support ($\sim$300 μm), YSZ electrolyte layer (20–30 μm), and porous YSZ layer ($\sim$70 μm) were stacked together under a vacuum condition and laminated at 20 MPa for 10 min using a thermal isostatic press (30T Shanxi, China) to form a NiO–YSZ supported tri-layer structure. The resulting tri-layer tape was punched to discs, and then co-sintered at 1,300 °C for 10 h in order to densify the electrolyte layer, during which graphite was burned out, leaving a well-formed porous YSZ network. The microstructural characteristics of the fired tri-layer tapes were performed using a scanning electron microscope, and the estimated porosity of the porous YSZ layer was 40 %–50 %.

A solution of LSM ((La$_{0.8}$Sr$_{0.2}$)$_{0.95}$MnO$_3$) precursor was prepared by dissolving stoichiometric amounts of La(NO$_3$)$_3 \cdot$6H$_2$O, Sr(NO$_3$)$_2$, Mn(NO$_3$)$_2$ (50 % w/w aqueous solution) into deionized water (Chen et al. 2012b). The solution was infiltrated into pre-treated porous YSZ layer and fired at 450 °C for 1 h to decompose the nitrate. In
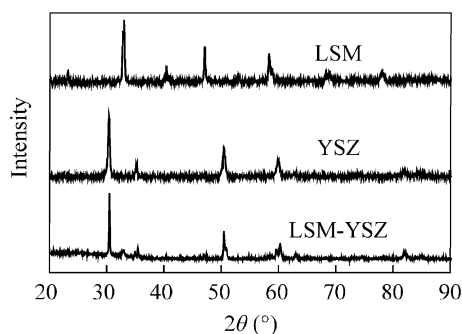
Fig. 1 X-ray diffraction patterns of LSM–YSZ oxygen electrode prepared by LSM infiltration method after sintering at 900 °C

order to ensure sufficient infiltration of LSM into the porous layer, repeated infiltration was used, followed by firing at 450 °C for 1 h after each infiltration. The infiltrated electrode was eventually fired at 900 °C for 2 h to reach a weight fraction of ~40 %. Ag paste (Beijing, China) was used as the current collector on electrode surfaces.

The RSOFCs were mounted on an alumina tube (Yu et al. 2005), sealed using ceramic paste as sealant (Aramco-552, USA) to separate the gas environment of the two electrodes, and tested in a tube furnace at temperatures from 800 to 850 °C. The area of electrolyte and hydrogen electrode was about 1.5 cm^2, the external area of oxygen electrode was 0.2 cm^2. For SOFC testing, 80 sccm flow rate of humidified hydrogen (3 vol% H_2O) was fed to the hydrogen electrode, while the oxygen electrode was exposed to ambient air. For SOEC operation, 50 % H_2O, 25 % H_2 and 25 % Ar were introduced into the Ni-based hydrogen electrode. Similarly, the oxygen electrode was left open to air. Polarization curves and electrochemical impedance spectra (EIS) under open circuit were conducted using an IM6 Electrochemical Workstation (ZAH-NER, Germany). For EIS test, the frequency range was from 100 mHz to 100 kHz, and the AC amplitude was 20 mV. Microstructure of the LSM-infiltrated RSOFC was examined using scanning electron microscopy (SEM, JEOL, JSM 6700F). In addition, the phase formation of LSM was examined using a high power X-ray diffractometer (XRD, PANalytical X'Pert PRO, Netherlands) with CuKα radiation.

3 Results and discussion

3.1 Physico-chemical characterization of RSOFCs

Figure 1 displays the XRD patterns of the LSM–YSZ oxygen electrode fabricated by infiltrating and sintered at 900 °C. In Fig. 1, the XRD patterns of pure perovskite
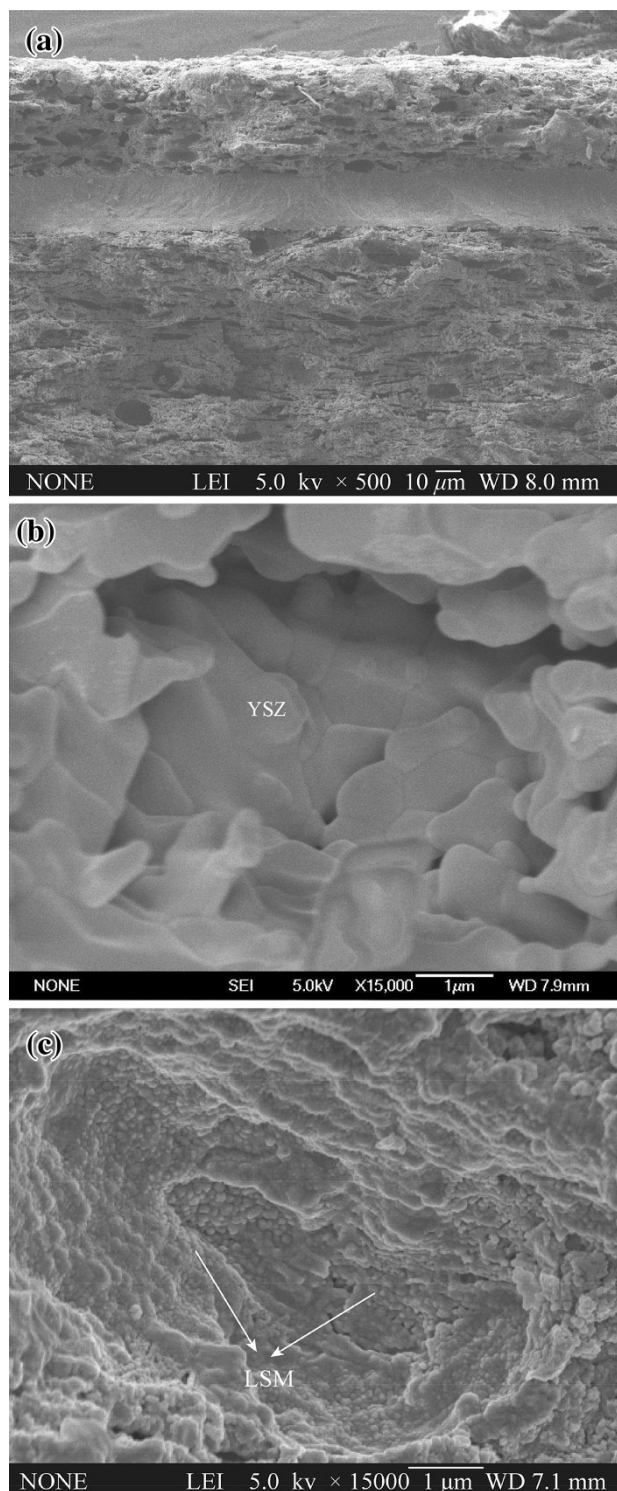
Fig. 2 Typical SEM images of cross-sectional view of **a** LSM-infiltrated NiO–YSZ/YSZ/LSM–YSZ single cell, **b** porous YSZ scaffold before infiltration and **c** LSM infiltrated LSM–YSZ oxygen electrode

LSM and YSZ are also shown as a reference. It is indicated that the infiltrated LSM–YSZ oxygen electrode has a mixture of perovskite LSM and YSZ phases, without

observable impurity phase. The LSM–YSZ oxygen electrode is therefore of high phase-purity.

A cross-sectional SEM of NiO–YSZ/YSZ/LSM–YSZ RSOFC is given in Fig. 2a. A dense YSZ electrolyte and porous electrode layers were observed. It is indicated that the co-sintering at 1,300 °C for 10 h forms dense YSZ electrolyte and porous YSZ electrode backbone. The thickness of cell components is ∼300, ∼20, and ∼60 μm for the hydrogen electrode, the electrolyte, and the oxygen electrode, respectively. Both the highly porous hydrogen and oxygen electrodes are in good contact with the dense electrolyte. Figure 2b and c are high-magnification SEM pictures focusing on the oxygen electrode before and after infiltration. In Fig. 2b, small grains of YSZ layer are formed at sintering temperature of 1,300 °C, and porosity for the porous YSZ layer is estimated at 40 %–50 % (Liu et al. 2010). Figure 2c reveals the microstructural feature of the LSM-infiltrated oxygen electrode. After infiltration and sintering, the submicro-sized LSM particles are uniformly and sufficiently covered on the pore walls of the YSZ network, forming a fairly densely packed microstructure to allow for sufficient electronic connectivity (Jiang et al. 2010). The small particle size of LSM is favorable for the catalytic activity of electrochemical reaction as well as the formation of more LSM/YSZ/gas TPB sites.

3.2 Initial electrochemical characterization under SOFC mode

Figure 3a shows the voltage and power density vs current density (V–I curve and P–I curve) at 850 and 800 °C for the LSM-infiltrated RSOFC. The open circuit voltage of the LSM-infiltrated cell is 1.065 V at 850 °C and 1.076 V at 800 °C, implying the YSZ electrolyte layer is fully dense after sintering at 1,300 °C and there is no leakage between the cell and the zirconia tube. The maximum power densities of the cell are ∼726 and ∼569 mW/cm² at 850 and 800 °C, respectively. In Fig. 3b, the ohmic impedance of the cell, determined from the high-frequency intercept on the real axis, was ∼0.24 Ω·cm² at 850 °C and ∼0.26 Ω·cm² at 800 °C. In addition, the polarization impedance of the cell, determined from the differences between high- and low-frequency intercepts on the impedance spectra, was 0.21 and 0.33 Ω·cm² at 850 and 800 °C, respectively. The high performance shown in infiltrated electrode is most likely due to the unique nanostructure fabricated at relatively low temperature (Sholklapper et al. 2006; Liu et al. 2010).

3.3 Electrochemical performance under SOEC mode

Figure 4a shows a high water electrolysis performance under SOEC mode at 850 and 800 °C for the LSM-
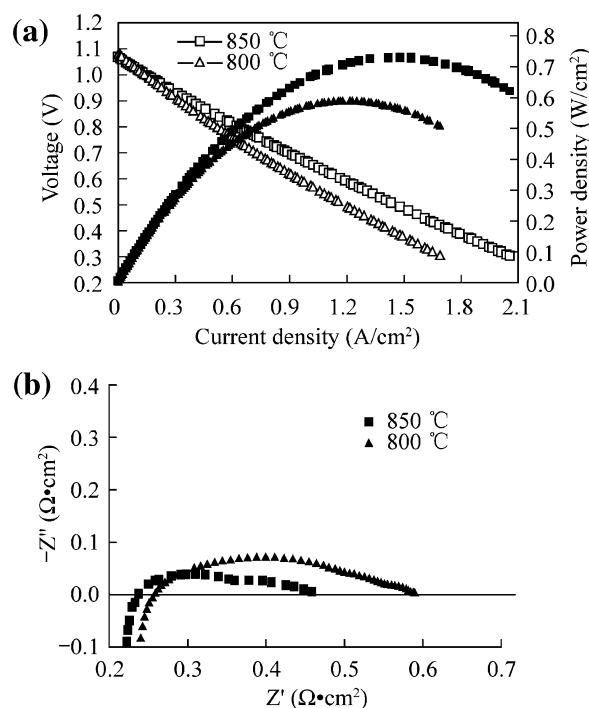
Fig. 3 a Voltage and power density vs current density, and **b** impedance spectrum at open circuit at 850 and 800 °C for LSM-infiltrated Ni–YSZ/YSZ/LSM–YSZ cell under SOFC mode operated with a 97 % H₂ and 3 % H₂O mixture at 80 sccm in the hydrogen electrode and ambient air in the oxygen electrode

infiltrated RSOFC, the input stream of 50 % H₂O, 25 % H₂ and 25 % Ar to hydrogen electrode and the air to oxygen electrode, respectively. The flow rate of inlet mixture gas was set as 150 sccm (standard cubic centimeters per minute). The electrochemical characteristic of LSM-infiltrated cell was recorded as a function of the operation temperature. The OCV of the cell was 0.906 V at 850 °C and 0.923 V at 800 °C. Both were near the theoretical OCV value calculated from Nernst formula (Liang et al. 2009; Laguna-Bercero et al. 2011). At 850 °C, the cell voltage for water electrolysis mode is only 1.35 V at 1 A/cm², and at 800 °C, the voltage is 1.47 V at 1 A/cm². At 850 and 800 °C, the electrochemical impedance spectra of LSM-infiltrated RSOFC under SOEC mode are measured at OCV, as shown in Fig. 4b. It can be seen that the electrode polarization losses decrease obviously with the increased operating temperature from 0.266 Ω·cm² at 800 °C to 0.158 Ω·cm² at 850 °C. The ohmic resistance shows no obvious change, from 0.272 Ω·cm² at 850 °C to 0.273 Ω·cm² at 800 °C. Yang et al. (2010) have reported that LSM-infiltrated cell has ohmic and polarization impedance smaller than those of the cell with LSM–YSZ electrode prepared by a mechanically mixing process and firing. The deposition of submicro-sized LSM on the porous YSZ network will effectively increase the number of the TPB sites for oxygen ion oxidation reaction. The LSM-infiltrated

(a)

(b)
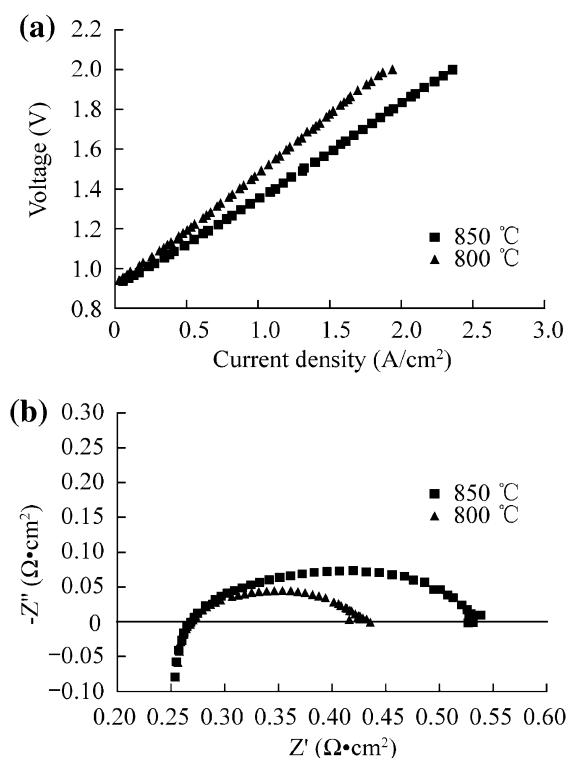
Fig. 4 **a** Voltage vs current density, and **b** impedance spectrum at open circuit at 850 and 800 °C for LSM-infiltrated Ni–YSZ/YSZ/LSM–YSZ cell under SOEC mode operated with a 50 % H_2O, 25 % H_2 and 25 % Ar gas mixture at 150 sccm in the hydrogen electrode and ambient air in the oxygen electrode

Fig. 5 Fuel cell/water electrolysis cycle of LSM-infiltrated Ni–YSZ/YSZ/LSM–YSZ cell at 800 °C and 400 mA/cm^2

electrode consequently has much lower polarization loss and higher performance.

3.4 Fuel cell/water electrolysis cycle

Charge/discharge cycle performance (1 h of water electrolysis and 1 h of fuel cell mode for each) of the LSM-infiltrated RSOFC at 800 °C is shown in Fig. 5. The cell has a slight performance loss during 6 cycles, with the discharge voltage decreased from 0.827 to 0.806 V and the charge voltage increased from 1.122 to 1.189 V at current density of 400 mA/cm^2, respectively. The larger voltage variation on charge than that on discharge is likely resulted from larger diffusion resistance of water molecules than that of hydrogen gas molecules for inlet gas mixture. However, the cell shows a small degradation rate of about 5 % or below after charge/discharge cycles. Thus, the LSM-infiltrated oxygen electrode can substantially avoid performance degradation and delamination from electrolyte, with good performance stability (Chen et al. 2012a).

4 Conclusions

In this study, porous LSM–YSZ oxygen electrode was prepared by infiltration process to fabricate Ni–YSZ/YSZ/LSM–YSZ RSOFC. X-ray diffraction and SEM analysis showed that perovskite phase LSM submicron particles were evenly distributed in the porous YSZ matrix. The electrochemical performance of the RSOFC was investigated in both fuel cell and water electrolysis modes at 800 and 850 °C. By infiltrating submicron-sized LSM into porous YSZ, the RSOFC cell performance has been significantly improved (Sholklapper et al. 2006). Under SOFC mode, the cell has a maximum power density of ~726 mW/cm^2, ohmic impedance of ~0.24 Ω·cm^2 and polarization impedance of 0.21 Ω·cm^2 at 850 °C. Under SOEC mode, the electrolysis voltage is 1.35 V at current density of 1 A/cm^2. Ohmic resistance is 0.272 Ω·cm^2 and polarization resistance is 0.158 Ω·cm^2 at 850 °C. Fuel cell/water electrolysis cycle performance shows that the cell has slight performance degradation during 6 cycles. Thereby, the LSM-infiltrated oxygen electrode has high electrochemical performance and good stability. It is concluded that the LSM–YSZ electrode made by infiltration process could be a promising oxygen electrode for high temperature RSOFC.

References

Chen KF, Jiang SP (2011) Failure mechanism of (La, Sr)MnO$_3$ oxygen electrodes of solid oxide electrolysis cells. Int J Hydrogen Energy 36:10541–10549

Chen GB, Zhang HM, Zhong HX, Ma HP (2010) Gas diffusion layer with titanium carbide for a unitized regenerative fuel cell. Electrochim Acta 55:8801–8807

Chen KF, Ai N, Jiang SP (2012a) Performance and stability of (La, Sr)MnO$_3$–Y$_2$O$_3$–ZrO$_2$ composite oxygen electrodes under solid oxide electrolysis cell operation conditions. Int J Hydrogen Energy 37:10517–10525

Chen KF, Ai N, Jiang SP (2012b) Reasons for the high stability of nano-structured (La, Sr)MnO$_3$ infiltrated Y$_2$O$_3$–ZrO$_2$ composite oxygen electrodes of solid oxide electrolysis cells. Electrochem Commun 19:119–122

Fu YP, Ouyang J, Li CH, Hu SH (2012) Characterization of nanosized Ce$_{0.8}$Sm$_{0.2}$O$_{1.9}$-infiltrated Sm$_{0.5}$Sr$_{0.5}$Co$_{0.8}$Cu$_{0.2}$O$_{3-\delta}$ cathodes for solid oxide fuel cells. Int J Hydrogen Energy 37:19027–19035

Gopalan S, Ye GS, Pal UB (2006) Regenerative, coal-based solid oxide fuel cell-electrolyzers. J Power Sources 162:74–80

Jiang SP (2012) Nanoscale and nano structured electrodes of solid oxide fuel cells by infiltration—advances and challenges. Int J Hydrogen Energy 37:449–470

Jiang ZY, Lei ZW, Ding B, Xia CR, Zhao F, Chen FL (2010) Electrochemical characteristics of solid oxide fuel cell cathodes prepared by infiltrating (La, Sr)MnO$_3$ nanoparticles into yttria-stabilized bismuth oxide backbones. Int J Hydrogen Energy 35:8322–8330

Jung GB, Chen JY, Lin CY, Sun SY (2012) Fabrication of hydrogen electrode supported cell for utilized regenerative solid oxide fuel cell application. Int J Hydrogen Energy 37:15801–15807

Keane M, Mahopatra MK, Verma A, Singh P (2012) LSM–YSZ interactions and anode delamination in solid oxide electrolysis cells. Int J Hydrogen Energy 37:16776–16785

Kiebach R, Knöfel C, Bozza F, Klemensø T, Chatzichristodoulou C (2013) Infiltration of ionic-, electronic- and mixed-conducting nano particles into LSM–YSZ cathodes—a comparative study of performance enhancement and stability at different temperatures. J Power Sources 228:170–177

Kim J, Ji HI, Dasari HP, Shin D, Song H, Lee JH, Kim BK, Je HJ, Lee HW, Yoon KJ (2013) Degradation mechanism of electrolyte and air electrode in solid oxide electrolysis cells operating at high polarization. Int J Hydrogen Energy 38:1225–1235

Kim-Lohsoontorn P, Brett DJL, Laosiripojana N (2010) Performance of solid oxide electrolysis cells based on composite La$_{0.8}$Sr$_{0.2}$MnO$_{3-\delta}$-yttria stabilized zirconia and Ba$_{0.5}$Sr$_{0.5}$Co$_{0.8}$Fe$_{0.2}$O$_{3-\delta}$ oxygen electrodes. Int J Hydrogen Energy 35:3958–3966

Knibbe R, Drennan J, Love JG (2009) Effect of alumina additions in YSZ on the microstructure and degradation of the LSM–YSZ interface. Solid State Ion 180:984–989

Laguna-Bercero MA, Kilner JA, Skinner SJ (2011) Development of oxygen electrodes for reversible solid oxide fuel cells with scandia stabilized zirconia electrolytes. Solid State Ionics 192:501–504

Liang MD, Yu B, Wen MF, Chen J, Xu JM, Zhai YC (2009) Preparation of LSM–YSZ composite powder for anode of solid oxide electrolysis cell and its activation mechanism. J Power Sources 190:341–345

Liu Z, Zheng ZW, Han MF, Liu ML (2010) High performance solid oxide fuel cells based on tri-layer yttria-stabilized zirconia by low temperature sintering process. J Power Sources 195:7230–7233

Rao YY, Wang ZQ, Zhong W, Peng RR, Lu YL (2012) Novel Ni–Ba$_{1+x}$Zr$_{0.3}$Ce$_{0.5}$Y$_{0.2}$O$_{3-\delta}$ hydrogen electrodes as effective reduction barriers for reversible solid oxide cells based on doped ceria electrolyte thin film. J Power Sources 199:142–145

Sholklapper TZ, Lu C, Jacobson CP, Visco SJ, Jonghe LCD (2006) LSM-infiltrated solid oxide fuel cell cathodes. Electrochem Solid-State Lett 9:A376–A378

Tao Y, Nishino H, Ashidate S, Kokubo H, Watanabe M, Uchida H (2009) Polarization properties of La$_{0.6}$Sr$_{0.4}$Co$_{0.2}$Fe$_{0.8}$O$_3$-based double layer-type oxygen electrodes for reversible SOFCs. Electrochim Acta 54:3309–3315

Virkar AV (2010) Mechanism of oxygen electrode delamination in solid oxide electrolyzer cells. Int J Hydrogen Energy 35:9527–9543

Yang CH, Jin C, Coffin A, Chen FL (2010) Characterization of infiltrated (La$_{0.75}$Sr$_{0.25}$)$_{0.95}$MnO$_3$ as oxygen electrode for solid oxide electrolysis cells. Int J Hydrogen Energy 35:5187–5193

Yu HC, Zhao F, Virkar AV, Fung KZ (2005) Electrochemical characterization and performance evaluation of intermediate temperature solid oxide fuel cell with La$_{0.75}$Sr$_{0.25}$CuO$_{2.5-\delta}$ cathode. J Power Sources 152:22–26